Acta Mech. Sin. (2012) 28(3):683–694
DOI 10.1007/s10409-012-0110-y

RESEARCH PAPER

On stability of elastic domain during isothermal solid–solid phase transformation in a tube configuration

Liang Dong · Qing-Ping Sun

Received: 24 November 2011 / Revised: 21 February 2012 / Accepted: 23 March 2012

Abstract Under isothermal quasi-static stretching the phase transition of a superelastic NiTi tube involves the formation (during loading) and vanishing (in unloading) of a high strain (martensite) domain. The two events are accompanied by a rapid stress drop/rise due to the formation/vanishing of domain fronts. From a thermodynamic point of view, both are instability phenomena that occur once the system reaches its critical state. This paper investigates the stability of a shrinking cylindrical domain in a tube configuration during unloading. The energetics and thermodynamic driving force of the cylindrical domain are quantified by using an elastic inclusion model. It is demonstrated that the two domain fronts exhibit strong interaction when they come close to each other, which brings a peak in the total energy and a sign change in the thermodynamic driving force. It is proved that such domain front interaction plays an important role in controlling the stability of the domain and in the occurrence of stress jumps during domain vanishing. It is also shown that the process is governed by two nondimensional length scales (the normalized tube length and normalized wall-thickness) and that the length scale dependence of the critical domain length and stress jump for the domain vanishing can be quantified by the elastic inclusion model.

Keywords Cylindrical elastic domain · Stability of domain · Domain front · Critical domain length · Stress jump · Thermodynamic driving force

The project was supported by the Hong Kong Research Grants Council (GRF619511) and from the National Natural Science Foundation of China (11128204).

L. Dong · Q. P. Sun (✉)
Department of Mechanical Engineering,
The Hong Kong University of Science and Technology
Clear Water Bay, Hong Kong, China
e-mail: meqpsun@ust.hk

1 Introduction

Due to its unique biocompatibility, shape memory and superelastic properties, NiTi shape memory alloy (SMA) tubes have obtained many important applications in the medical device industry, ranging from catheters to superelastic needles, from small-scale self-expanding endovascular stents to other implantable structures (see, for example Refs. [1, 2]). In these applications, a comprehensive knowledge of thermomechanical behaviors of the material is needed. Research on the deformation behavior of NiTi tubes during phase transition under tensile loading started only in recent years (among many others, see Refs. [3–17]). The study was partially motivated by the rapid growth of mechanical engineers' interest in NiTi tubes and the related devices which are subjected to a wide range of loading conditions in service, and partially motivated by our curiosity about the phase transition and domain evolution in the polycrystalline tube geometry, the origins of its nonlinear and multi-field coupling and the resulting deformation patterns and the length scales [17–28]. From a pure academic point of view, the tube configuration is also an interesting and convenient system in investigating phase transition behaviors of the material.

One of the key aspects in phase transition behaviors of the NiTi tube under tension is the dynamic martensite band formation/vanishing which is accompanied by a rapid stress drop/jump. The phenomena are widely observed in tubes with an arbitrary wall-thickness/mean-radius ratio ranging from 0 to 2 (i.e., from a very thin tube to an extreme case of a solid wire). The experiment of a long tube (with tube length/mean-radius ratio $\approx$ 270 and wall-thickness/mean-radius ratio = 0.5) under quasi-static isothermal stretching (with applied strain rate 5×10^{-4} s^{-1}) is shown in Fig. 1a. It can be seen that at a critical stress the initial homogeneous deformation (Fig. 1a, A) of the tube (in the austenite phase) suffers instability and self-organizes into a mixture of a low-strain matrix (austenite phase) and a high-strain cylindrical martensite band (Fig. 1a, B) with a sudden stress drop. The subsequent phase transition of the tube is realized through

the growth and shrinkage of the cylinder-shaped band at the respective upper and lower stress plateaus (see B-C and E-G in Fig. 1a). During unloading, when the martensite domain length is reduced to a critical value, the domain dynamically vanishes with a steep stress jump (Fig. 1a, G-H) which is much smaller than the stress drop during the domain formation (Fig. 1a, A-B). While for a short wire (with wire length/mean-radius ratio = 15 and wall-thickness/mean-radius ratio = 2) under the same loading condition as shown in Fig. 1b, the stress jump (Fig. 1b, H-I) during the domain vanishing can be significant (about a half of the stress drop in the domain formation, see A-B in Fig. 1b). From a thermodynamic point of view, both the domain formation and vanishing are instability events occurring once the system reaches its critical state, in order to understand and model the instability in domain formation/vanishing, the energetics and stability of domain need to be explored.

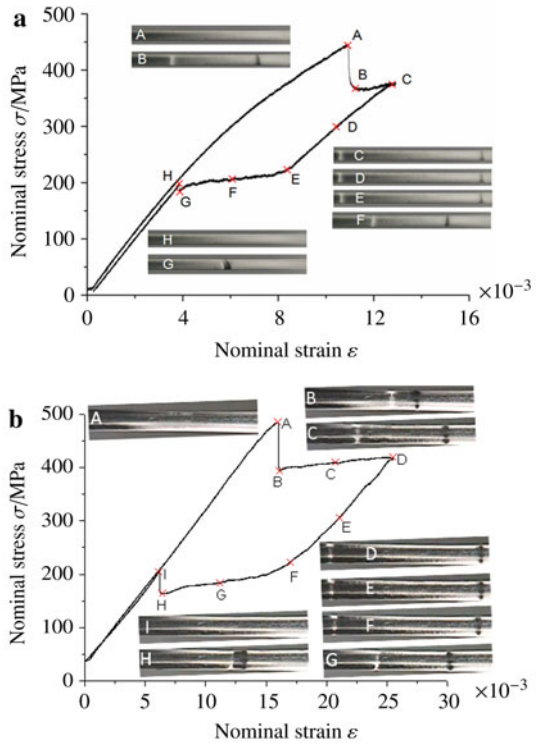

Fig. 1 The synchronized stress-strain response and the surface morphologies of **a** a long tube (with tube length/mean-radius ratio ≈ 270 and wall-thickness/mean-radius ratio = 0.5) and **b** a solid wire (with wire length/mean-radius ratio = 15 and wall-thickness/mean-radius ratio = 2) under quasi-static tensile loading and unloading

A systematic and quantitative study is necessary for investigating the stress fields, strain energy distribution and their evolution in the tube. Among many other factors (defect, microstructure, external noise, etc.), the domain front interaction plays the most important role in the energetics of the unstable events. The following issues must be clarified before the modeling of the martensite domain. Firstly, the domain consists of almost fully transformed grains whose statistical average transformation strains (eigenstrains) under uniaxial tension are constants (5%, –2.5% and –2.5% in axial, radial and circumferential directions). Thus the domain can be treated approximately as an elastic inclusion, but it is non-classic since the domain is not fully constrained by the matrix [29–31]. However, the theoretical principle and method to solve the problem are the same as those for the classical inclusion-matrix system [32]. Secondly, the domain can nucleate into different patterns in tubes of different wall-thickness/mean-radius ratios, e.g., it can be a helix in thin-walled tubes and a cylinder in thick-walled tubes [4, 5, 8–10, 15–17]. In all the thin-walled tubes, further loading will make the helical domain grow and eventually merge into a cylindrical domain. During unloading the reverse transition of the cylindrical domain is realized by the reverse propagation of its fronts and the final dynamic domain vanishing. Compared with the more complex helical domains, analysis of the vanishing process of the cylindrical domain is relatively simple and will be a good example for the investigation of the domain stability as well as stable → unstable transition of an existing domain. Thirdly, it is noticed that even a cylindrical domain can have different equilibrium front morphologies such as the inclined fronts, perpendicular fronts or branched fronts [10].

The objective of this paper is to study the stability of a cylindrical martensite domain during its isothermal shrinkage in the unloading process. The domain is treated as an elastic inclusion in the tube configuration, and the domain fronts are assumed to be perpendicular to the loading axis mainly for the purpose of mathematical simplicity. Focus is concentrated on the energetics and thermodynamic driving force during the domain evolution so that the stress jump phenomenon in domain vanishing can be explained and quantified. The paper is organized as follows. In Sect. 2, the domain front interaction is quantitatively examined for a thin-walled tube. Based on the calculations of misfit energy and thermodynamic driving force in Sect. 2, the stability of the martensite domain under displacement-controlled unloading is discussed in Sect. 3. In Sect. 4, the discussions of domain stability are extended to the more general cases of arbitrary wall-thickness. The summary and conclusions are given in Sect. 5.

2 Domain front interaction

Consider a cylindrical tube with length L and a uniform cross section of mean-radius R and wall-thickness t in the cylindrical coordinate system as shown in Fig. 2a. The tube contains a cylindrical martensite domain Ω of length L_{M} with constant axisymmetric (with respect to the z-axis) eigenstrain $\varepsilon^{\mathrm{p}}_{ij}$ (with non-zero components $\varepsilon^{\mathrm{p}}_{r}$, $\varepsilon^{\mathrm{p}}_{\theta}$ and $\varepsilon^{\mathrm{p}}_{z}$). The elastic constants of the domain and the matrix are assumed to be isotropic and are the same. For most shape memory alloys, the volume change in phase transformation is ignorable and

these nonzero components of transformation strain can be written as

$$\varepsilon_r^{\mathrm{p}} = \varepsilon_\theta^{\mathrm{p}} = \varepsilon_1^{\mathrm{p}} < 0, \quad \varepsilon_z^{\mathrm{p}} = \varepsilon_2^{\mathrm{p}} = -2\varepsilon_1^{\mathrm{p}} > 0. \tag{1}$$

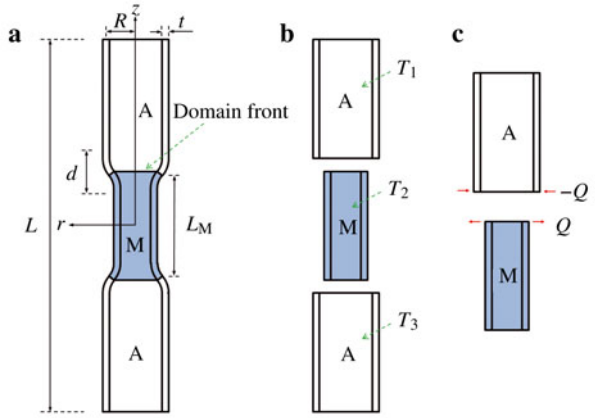

Fig. 2 Schematic diagram of the overall necking deformation in the tube. **a** Real mode; **b** Disconnected stress-free mode; **c** Connecting forces joining T_1 and T_2

Remark 1: In real martensitic transformation in SMA, the Young's modulus of martensite is usually less than that of austenite, so to be exact the martensite domain should be treated as an inhomogeneous inclusion [32]. The assumption in Eq. (1) is based on the experimental measurement of the statistical average strain of numerous grains in the fully transformed region. It should be noticed that a possible texture might invalidate the assumption of two equal components of the transformation strain. Moreover, in a real polycrystalline material, the transformation strain (or volume fraction of martensite) may change continuously and rapidly across the domain front (i.e., the boundary zone). In other words, the domain front has a finite thickness. Here the constant or uniform transformation strain assumption is used mainly for the purpose of simplicity.

For a long thin-walled tube ($L \gg R \gg t$), its deformation arising from the presence of a cylindrical martensite domain can be represented by the deflection, w, of the tube's mid-surface. If both ends of the tube are free from any external constraint, the equilibrium configuration of the tube is determined by the minimization of the total energy (or total misfit energy) which contains two energy terms, pure bending energy and stretching energy [33]. Pure bending energy arises from the non-uniformity of tension and compression through the wall-thickness of the tube, while the stretching energy is due to the general mid-surface stretching. When the distance between the two fronts (i.e., the domain length) becomes large enough, the pure bending and stretching energies will no longer depend on L_{M}. The resultant total misfit energy of the system can be generally expressed as $U_{\mathrm{el}} \sim Et^{3/2}w^2/R^{1/2}$ and the characteristic length scale d of the necking (bending) zone (see Fig. 2a) can be determined as $d \sim \sqrt{Rt}$ (see Appendix I for detailed derivation).

From the elementary theory of elasticity [34], an analytical expression of the total misfit energy of the system due to the presence of a long martensite domain (without the interaction of two fronts) can be obtained as

$$U_{\mathrm{el}} = \frac{1}{2}\pi RtE\left(\varepsilon_1^{\mathrm{p}}\right)^2 d, \tag{2}$$

where $d = [R^2t^2/3(1-\nu^2)]^{1/4}$ is a constant for a given tube mean-radius and wall-thickness.

The stress and strain fields associated with each domain front will interact with each other when the domain length becomes comparable to or less than the necking zone length (i.e., $L_{\mathrm{M}} \sim d$). The total misfit energy of the system now depends on the domain length L_{M} and can be expressed as

$$U_{\mathrm{el}} = \frac{1}{2}\pi RtE\left(\varepsilon_1^{\mathrm{p}}\right)^2 d\left(1 - \mathrm{e}^{-L_{\mathrm{M}}/d}\cos\frac{L_{\mathrm{M}}}{d} + \mathrm{e}^{-L_{\mathrm{M}}/d}\sin\frac{L_{\mathrm{M}}}{d}\right). \tag{3}$$

It is seen from Eqs. (2) and (3) that the total misfit energy depends on three length scales: the domain length L_{M}, mean-radius R and wall-thickness t of the tube. The mean-radius and wall-thickness determine the characteristic length scale d of the necking zone which stores the bending and stretching energies. For a given R and t, the domain length L_{M} determines the front interaction which occurs when the domain length becomes comparable to or less than the necking zone length.

The thermodynamic driving force, i.e., the material or configurational force, at a sharp interface (domain front) has been discussed in many notable papers [35–44]. The driving force for the interface (domain front) motion can be obtained as

$$f = -\frac{\mathrm{d}U}{\mathrm{d}L_{\mathrm{M}}}. \tag{4}$$

where U is the Helmholtz free energy of the system for displacement-controlled loading and is the Gibbs free energy of the system for force-controlled loading.

For the current case, $U = U_{\mathrm{el}}$. By substituting Eq. (3) into Eq. (4),

$$f_{\mathrm{el}} = -\frac{\mathrm{d}U_{\mathrm{el}}}{\mathrm{d}L_{\mathrm{M}}} = -\pi RtE\left(\varepsilon_1^{\mathrm{p}}\right)^2 \mathrm{e}^{-L_{\mathrm{M}}/d}\cos\frac{L_{\mathrm{M}}}{d}. \tag{5}$$

Theoretical calculations of the variations of U_{el} and f_{el} with L_{M} for the case $t/R = 0.1$ are shown in Fig. 3, from which the front interaction can be seen clearly. For a large domain length ($L_{\mathrm{M}}/R > 2$), the elastic misfit energy U_{el} is a constant (see Fig. 3a). As the domain length L_{M} decreases, the elastic misfit energy U_{el} first increases gradually to a peak (Point 1) and then decreases to zero. Accordingly in Fig. 3b, for a large domain length ($L_{\mathrm{M}}/R > 2$), the driving force f_{el} is zero, which means the two interfaces have no interaction. As L_{M} decreases, the driving force f_{el} becomes positive, which

means that two interfaces repel each other and the growth of the elastic domain is favored. There exists a critical domain length $L_{\mathrm{M}}^{\mathrm{c}}$ (Point 1 in Fig. 3b) below which the driving force f_{el} becomes negative and favors the shrinkage of the martensite domain. It should be noticed that such a critical domain length $L_{\mathrm{M}}^{\mathrm{c}}$ coincides with the peak in the misfit energy (Point 1 in Fig. 3a). The magnitude of the driving force increases monotonically as L_{M} decreases and reaches its maximum at the end of domain vanishing (L_{M}= 0) which makes domain vanishing a dynamic process. The maximum positive driving force (Point 2 in Fig. 3b) corresponds to the turning point (Point 2 in Fig. 3a) of the misfit energy.

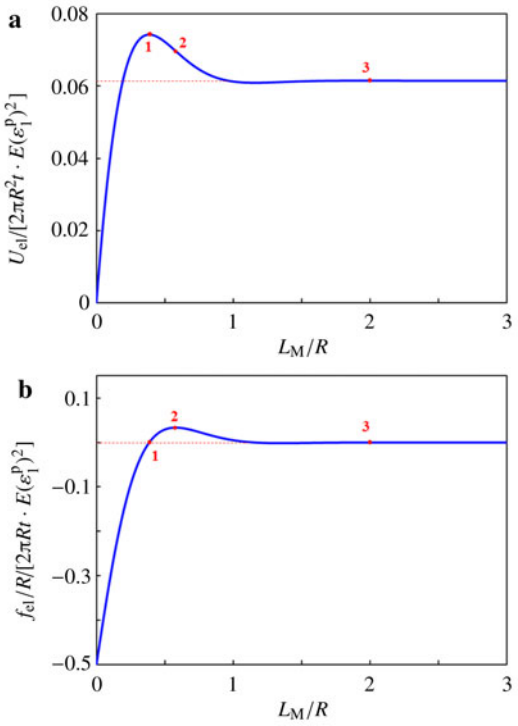

Fig. 3 Variation of **a** elastic misfit energy U_{el} and **b** thermodynamic driving force f_{el} with the domain length L_{M} for $t/R = 0.1$ (thin-walled tube)

3 Stability of domain

Based on the calculations of the misfit energy and thermodynamic driving force in Sect. 2, we study the stability of a martensite domain in a thin-walled tube (with $t/R = 0.1$) during the displacement-controlled unloading. For this problem there are five external governing parameters, with three geometric parameters (the wall-thickness t, mean-radius R and length L of the tube) and two loading parameters (the applied nominal strain ε_0 (= tube-elongation/tube-length) and the temperature T). The domain length L_{M} is an internal variable which characterizes the phase transition process. The Helmholtz free energy of the system under displacement-controlled boundary conditions can be expressed as [29]

$$U = U_{\mathrm{el}} + \Delta U_{\mathrm{chem}} + U_{\mathrm{ext}}, \tag{6}$$

where ΔU_{chem} is the change in chemical free energy, U_{el} is the misfit strain energy arising from the presence of martensite domain and U_{ext} is the extra elastic energy arising from the external displacement-controlled stretching.

Taking the stress-free austenite phase as the reference state, the total change in chemical free energy arising from the thermo-elastic martensitic transformation is

$$\Delta U_{\mathrm{chem}} = \int_{\Omega} \Delta\varphi \mathrm{d}V = V_{\Omega}\Delta\varphi(T) = 2\pi RtL_{\mathrm{M}}\Delta\varphi(T), \tag{7}$$

where $\Delta\varphi(T)$ is the chemical free energy density difference between the two phases. It depends only on the temperature T and can be approximated as a linear function of T around the equilibrium temperature T_0

$$\Delta\varphi(T) = \varphi^{\mathrm{M}}(T) - \varphi^{\mathrm{A}}(T) = k(T - T_0), \tag{8}$$

where k is a material constant determined by the experiments.

The extra elastic energy arising from external displacement-controlled loading can be expressed as

$$U_{\mathrm{ext}} = \pi RtLE\left(\varepsilon_0 - \frac{L_{\mathrm{M}}\varepsilon_2^{\mathrm{p}}}{L}\right)^2. \tag{9}$$

For the given tube geometry (tube wall-thickness t, mean-radius R and length L) and the given temperature T, there are only two parameters (domain length L_{M} and nominal strain ε_0) that control the phase transition process and the stability of the martensite domain. The purpose of this paper is to investigate the stability of the equilibrium domain in a displacement-controlled process, i.e., for equilibrium domain at any given nominal strain. Therefore, it is appropriate for us to conduct stability analysis by treating the Helmholtz free energy as a function of the domain length L_{M} subject to the given nominal strain ε_0. As for the force-controlled process, the stability of the martensite domain can be similarly considered by employing the Gibbs free energy of the system.

Under isothermal and quasi-static conditions, the driving force for the interface motion can be obtained for the displacement-controlled loading condition as

$$f = -\left.\frac{\mathrm{d}U}{\mathrm{d}L_{\mathrm{M}}}\right|_{\varepsilon_0} = f_{\mathrm{el}} + f_{\mathrm{chem}} + f_{\mathrm{ext}}, \tag{10}$$

where f_{el} for a thin-walled tube is given in Eq. (5) as

$$f_{\mathrm{el}} = -\frac{\mathrm{d}U_{\mathrm{el}}}{\mathrm{d}L_{\mathrm{M}}} = -\pi RtE\left(\varepsilon_1^{\mathrm{p}}\right)^2 \mathrm{e}^{-L_{\mathrm{M}}/d}\cos\frac{L_{\mathrm{M}}}{d},$$

and

$$f_{\mathrm{chem}} = -\frac{\mathrm{d}\Delta U_{\mathrm{chem}}}{\mathrm{d}L_{\mathrm{M}}} = -2\pi Rt\Delta\varphi, \tag{11}$$

$$f_{\mathrm{ext}} = -\left.\frac{\mathrm{d}U_{\mathrm{ext}}}{\mathrm{d}L_{\mathrm{M}}}\right|_{\varepsilon_0} = 2\pi RtE\varepsilon_2^{\mathrm{p}}\left(\varepsilon_0 - \frac{L_{\mathrm{M}}\varepsilon_2^{\mathrm{p}}}{L}\right). \tag{12}$$

Consider the quasi-static unloading with displacement-controlled boundary condition (by monotonically decreasing the nominal strain ε_0). The energy dissipation of the phase transition in SMA can be accounted for by introducing a constant dry-friction force D_0 [29]. By imposing condition $f = -D_0$ on the reverse phase transition and referring to Eq. (10), we find the relation between the nominal strain ε_0 and the domain length L_M as

$$\varepsilon_0 = \frac{L_\mathrm{M}\varepsilon_2^\mathrm{p}}{L} + \frac{1}{8}\mathrm{e}^{-L_\mathrm{M}/d}\varepsilon_2^\mathrm{p}\cos\frac{L_\mathrm{M}}{d} + \frac{\Delta\varphi - D_0}{E\varepsilon_2^\mathrm{p}}. \tag{13}$$

The corresponding nominal stress can be given by

$$\begin{aligned}\sigma_0 &= E\left(\varepsilon_0 - \frac{L_\mathrm{M}\varepsilon_2^\mathrm{p}}{L}\right)\\ &= \frac{1}{8}\mathrm{e}^{-L_\mathrm{M}/d}E\varepsilon_2^\mathrm{p}\cos\frac{L_\mathrm{M}}{d} + \frac{\Delta\varphi - D_0}{\varepsilon_2^\mathrm{p}}.\end{aligned} \tag{14}$$

Remark 2: It should be noted that in general the energy minimization principle should not be applied directly to the above irreversible process with energy dissipation. However, as argued in Refs. [4, 45] and much earlier by Rice [46], for the constrained equilibrium studied in this paper both the chemical energy difference $\Delta\varphi$ and the dry-friction force D_0 can be chosen as zero without losing generality. It can be seen from Eqs. (15) and (18) below that the values of $\Delta\varphi$ and D_0 have no effect either on the critical domain length L_M^c or on the stress jump $\Delta\sigma$. It can also be seen from Eq. (13) that $\Delta\varphi$ and D_0 affect the values of the critical nominal strain ε_0^c by a constant only.

If the driving force f (Eq. (10)) equals zero at a given ε_0, the Helmholtz free energy of the system reaches a stationary point (i.e., a local maximum, a local minimum or a saddle point), then the stability of the martensite domain can be determined by the second derivative κ of the Helmholtz free energy

$$\begin{aligned}\kappa &= \frac{\mathrm{d}^2U}{\mathrm{d}L_\mathrm{M}^2}\\ &= 2\pi RtE\left(\varepsilon_1^\mathrm{p}\right)^2\left[-\frac{1}{2d}\mathrm{e}^{-L_\mathrm{M}/d}\left(\cos\frac{L_\mathrm{M}}{d} + \sin\frac{L_\mathrm{M}}{d}\right)\right.\\ &\quad\left. + \frac{1}{L}\left(\frac{\varepsilon_2^\mathrm{p}}{\varepsilon_1^\mathrm{p}}\right)^2\right].\end{aligned} \tag{15}$$

In principle, if $\kappa > 0$ at the domain length L_M corresponding to $f = 0$, the Helmholtz free energy U reaches a local minimum point, which means that the equilibrium domain is stable. If $\kappa < 0$, the Helmholtz free energy stays at a local maximum point so the equilibrium domain is unstable. If $\kappa = 0$ and its sign changes across such a point, the Helmholtz free energy corresponds to a saddle point (or spinodal point, i.e., a point that is stationary but not a local extremum) [47, 48] at which the domain is also unstable. The variations of the second derivative κ with the domain length L_M for different tube length L are shown in Fig. 4. It is seen that for relatively large domain lengths, the second derivative κ is always positive. It changes its sign at a critical domain lengths L_M^c, which corresponds to the saddle point of the system energy. It is also seen that the critical domain length L_M^c increases as the tube length L increases and there is a limit $L_\mathrm{M}^\mathrm{c}/R \approx 0.58$ when L/R approaches infinity.

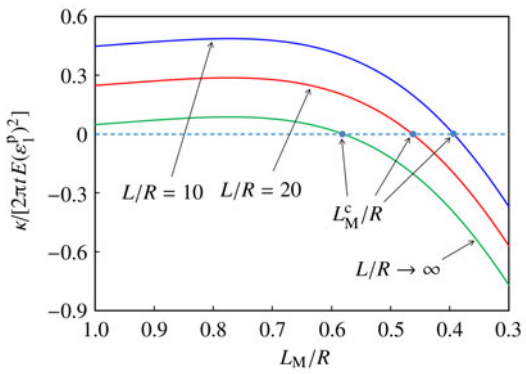

Fig. 4 Variation of the second derivative κ of the Helmholtz free energy with the domain length L_M for different tube lengths L

As shown in Fig. 5, the model has the capability to capture the instability event which occurs in the quasi-static unloading process: as the nominal strain ε_0 decreases, the equilibrium domain is stable and its length L_M decreases monotonically until a critical state with $\varepsilon_0 = \varepsilon_0^\mathrm{c}$ and $L_\mathrm{M} = L_\mathrm{M}^\mathrm{c}$ is reached. The energetics of the equilibrium domains in the strain range $\varepsilon_0 > \varepsilon_0^\mathrm{c}$ is shown in Fig. 5(I). It is seen that the equilibrium domain length corresponds to a local minimum of the system energy (accordingly with $\kappa > 0$ as shown in Fig. 4) and thus the martensite→austenite phase transition is stable. However, the system energy at the critical state (with $\varepsilon_0 = \varepsilon_0^\mathrm{c}$ and $L_\mathrm{M} = L_\mathrm{M}^\mathrm{c}$) stays at a spinodal point (with $\kappa = 0$, see Fig. 4) and is shown in Fig. 5(II). The system energy will monotonically decrease when the domain length decreases. Therefore, the equilibrium martensite domain at the critical state (with $\varepsilon_0 = \varepsilon_0^\mathrm{c}$ and $L_\mathrm{M} = L_\mathrm{M}^\mathrm{c}$) is unstable, which means that the domain length will decrease rapidly leading to dynamic domain vanishing. The dashed lines in Fig. 5 correspond to those unstable equilibrium states (with $\kappa < 0$ as shown in Fig. 4).

At the critical nominal strain $\varepsilon_0 = \varepsilon_0^\mathrm{c}$, the variation of the total driving force $f = f_\mathrm{el} + 2\pi RtE\varepsilon_2^\mathrm{p}(\varepsilon_0^\mathrm{c} - L_\mathrm{M}\varepsilon_2^\mathrm{p}/L)$ with the domain length L_M is shown in Fig. 6. It is seen that the driving force is always negative and decreases as L_M decreases. Therefore, it can be concluded that the martensite domain becomes unstable at the critical nominal strain ε_0^c and any small change in the domain length will cause domain vanishing.

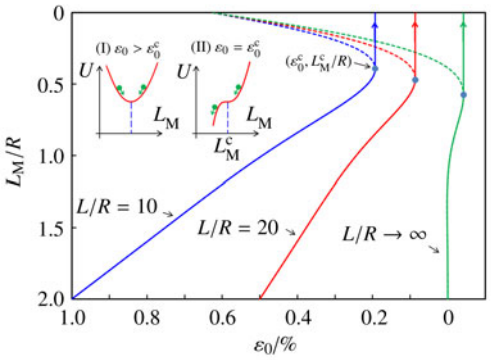

Fig. 5 Variation of the equilibrium domain length L_M with the nominal strain ε_0 for different tube lengths L (for $\Delta\varphi = 0$ and $D_0 = 0$). The energetics is shown in (I) for the stable state (with $\varepsilon_0 > \varepsilon_0^c$) and (II) for the critical state (with $\varepsilon_0 = \varepsilon_0^c$)

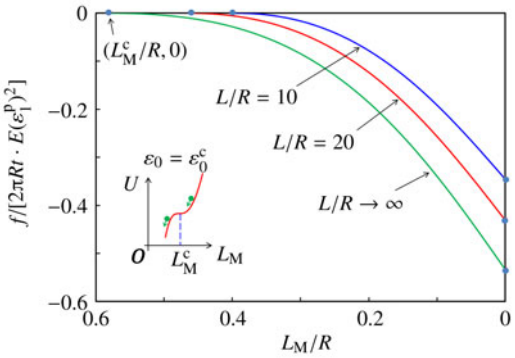

Fig. 6 Variation of the total driving force f with the domain length L_M at the critical nominal strain ε_0^c for different tube lengths L

The variation of the nominal stress σ_0 with the nominal strain ε_0 for different tube lengths L is plotted in Fig. 7. It is seen that at large nominal strain the nominal stress σ_0 is zero (since we take $\Delta\varphi = 0$ and $D_0 = 0$). As the nominal strain ε_0 decreases, the nominal stress σ_0 first decreases gradually and then increases until the critical state is reached at which unstable domain vanishing happens. Accompanying the domain vanishing is a sudden jump in the nominal stress. The elastic strain immediately before the domain vanishing is

$$\varepsilon_e^{c-} = \varepsilon_0^c - \frac{L_M^c \varepsilon_2^p}{L} = \frac{1}{8} e^{-L_M^c/d} \varepsilon_2^p \cos\frac{L_M^c}{d} + \frac{\Delta\varphi - D_0}{E\varepsilon_2^p} \tag{16}$$

and the elastic strain following the domain vanishing is

$$\varepsilon_e^{c+} = \varepsilon_0^c = \frac{L_M^c \varepsilon_2^p}{L} + \frac{1}{8} e^{-L_M^c/d} \varepsilon_2^p \cos\frac{L_M^c}{d} + \frac{\Delta\varphi - D_0}{E\varepsilon_2^p}. \tag{17}$$

Therefore, the corresponding stress jump in the domain vanishing can be given by

$$\Delta\sigma = E\left(\varepsilon_e^{c+} - \varepsilon_e^{c-}\right) = \frac{L_M^c E \varepsilon_2^p}{L}. \tag{18}$$

It is seen that the stress jump is linearly proportional to the critical domain length L_M^c and inversely proportional to the tube length L. It should be noted that the stress jump is always positive since the critical domain length L_M^c is always positive. Especially, the stress jump approaches zero when $L/R \to \infty$.

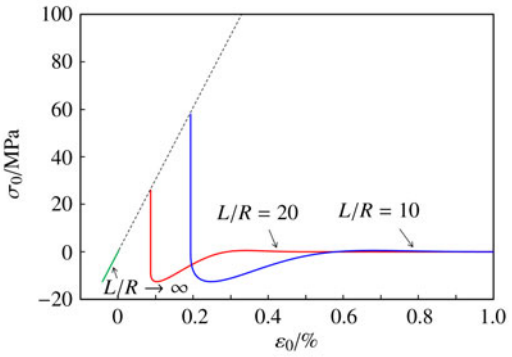

Fig. 7 Variation of the nominal stress σ_0 with the nominal strain ε_0 for different tube lengths L

In summary, unstable domain vanishing happens at the critical domain length L_M^c during the displacement-controlled unloading. This critical domain length L_M^c is determined by the tube geometry (wall-thickness t, mean-radius R and length L). For a tube with a given normalized wall-thickness t/R, as the tube length L/R increases the critical domain length L_M^c/R increases monotonically while the corresponding stress jump $\Delta\sigma$ decreases monotonically.

4 Three-dimensional problems

The discussions in Sect. 3 for the thin-walled tube ($t/R = 0.1$) can be extended to tubes with an arbitrary wall-thickness by solving a three-dimensional inclusion problem. For this general problem in the cylindrical coordinates, the displacement component u_θ vanishes and u_r, u_z are independent of θ. The nonzero strain components are

$$\varepsilon_r = \frac{\partial u_r}{\partial r}, \quad \varepsilon_\theta = \frac{u_r}{r}, \quad \varepsilon_z = \frac{\partial u_z}{\partial z}, \quad \varepsilon_{rz} = \frac{1}{2}\left(\frac{\partial u_r}{\partial z} + \frac{\partial u_z}{\partial r}\right). \tag{19}$$

The corresponding stress components can be given by

$$\begin{aligned}
\sigma_r &= \frac{E}{1+v}\left[\frac{v\,(e - e^p)}{1-2v} + \varepsilon_r - \varepsilon_r^p\right],\\
\sigma_\theta &= \frac{E}{1+v}\left[\frac{v\,(e - e^p)}{1-2v} + \varepsilon_\theta - \varepsilon_\theta^p\right],\\
\sigma_z &= \frac{E}{1+v}\left[\frac{v\,(e - e^p)}{1-2v} + \varepsilon_z - \varepsilon_z^p\right],\\
\sigma_{rz} &= \frac{E\varepsilon_{rz}}{1+v}, \quad \text{for} \quad |z| < \frac{L_M}{2},\\
\sigma_r &= \frac{E}{1+v}\left(\frac{ve}{1-2v} + \varepsilon_r\right), \quad \sigma_\theta = \frac{E}{1+v}\left(\frac{ve}{1-2v} + \varepsilon_\theta\right),\\
\sigma_z &= \frac{E}{1+v}\left(\frac{ve}{1-2v} + \varepsilon_z\right),\\
\sigma_{rz} &= \frac{E\varepsilon_{rz}}{1+v}, \quad \text{for} \quad |z| > \frac{L_M}{2},
\end{aligned} \tag{20}$$

where $e = \varepsilon_r + \varepsilon_\theta + \varepsilon_z$ and $e^{\mathrm{p}} = \varepsilon_r^{\mathrm{p}} + \varepsilon_\theta^{\mathrm{p}} + \varepsilon_z^{\mathrm{p}}$.

Moreover, the stress components in the inclusion and the matrix satisfy the following equations of equilibrium

$$\frac{\partial \sigma_r}{\partial r} + \frac{\partial \sigma_{rz}}{\partial z} + \frac{\sigma_r - \sigma_\theta}{r} = 0, \quad \frac{\partial \sigma_{rz}}{\partial r} + \frac{\partial \sigma_z}{\partial z} + \frac{\sigma_{rz}}{r} = 0. \quad (21)$$

Substituting Eq. (20) into Eq. (21), we obtain the Navier equations for the displacements

$$\frac{1}{1-2\nu}\frac{\partial e}{\partial r} + \nabla^2 u_r - \frac{u_r}{r^2} = 0, \quad \frac{1}{1-2\nu}\frac{\partial e}{\partial z} + \nabla^2 u_z = 0, \quad (22)$$

where $\nabla^2 = \partial^2/\partial r^2 + 1/r \cdot \partial/\partial r + \partial^2/\partial z^2$.

The stress-free boundary conditions on the inner and outer surfaces are

$$\sigma_r = \sigma_{rz} = 0, \ \text{ for } \ r = R \pm \frac{t}{2}. \quad (23)$$

The solution for the stress and strain energy in the tube can be decomposed into the solutions of two sub-problems as shown in Fig. 8. In Sub-problem 1, the martensite domain (with constant eigenstrains $\varepsilon_r^{\mathrm{p}}$, $\varepsilon_\theta^{\mathrm{p}}$ and $\varepsilon_z^{\mathrm{p}}$) is subjected to the traction $p = -E\varepsilon_1^{\mathrm{p}}/(1-\nu) > 0$ on its inner and outer surfaces to guarantee that there is no radial deflection of the tube. In Sub-problem 2, the pure elastic tube deforms under the pressure $p = -E\varepsilon_1^{\mathrm{p}}/(1-\nu) > 0$ prescribed on the inner and outer surfaces which has the same magnitude as but opposite direction to those in Sub-problem 1. Details of the solution are given in Appendix II., readers are referred to works [29–31] for more details.

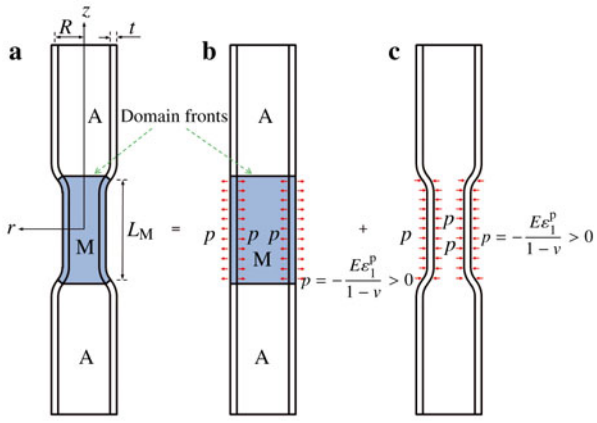

Fig. 8 Decomposition of the original problem into two sub-problems. **a** Original problem; **b** Sub-problem 1; **c** Sub-problem 2

The elastic misfit energy of the tube due to the presence of the martensite domain, according to the inclusion theory [32], can be generally expressed as

$$U_{\mathrm{el}} = -\frac{1}{2}\int_\Omega \sigma_{ij}\varepsilon_{ij}^{\mathrm{p}} dV = -\frac{1}{2}\left(\bar{\sigma}_r\varepsilon_r^{\mathrm{p}} + \bar{\sigma}_\theta\varepsilon_\theta^{\mathrm{p}} + \bar{\sigma}_z\varepsilon_z^{\mathrm{p}}\right)V_\Omega, \quad (24)$$

where $\bar{\sigma}_r$, $\bar{\sigma}_\theta$ and $\bar{\sigma}_z$ denote respectively the average of stress σ_r, σ_θ and σ_z over the inclusion (domain) Ω

$$\begin{aligned} \bar{\sigma}_r &= \frac{1}{V_\Omega}\int_\Omega \sigma_r \mathrm{d}V, \\ \bar{\sigma}_\theta &= \frac{1}{V_\Omega}\int_\Omega \sigma_\theta \mathrm{d}V, \\ \bar{\sigma}_z &= \frac{1}{V_\Omega}\int_\Omega \sigma_z \mathrm{d}V. \end{aligned} \quad (25)$$

By substituting Eqs. (A6), (A11) and (A14) into Eq. (25), we obtain

$$\bar{\sigma}_r + \bar{\sigma}_\theta = \frac{2}{1-\nu}H\left(\frac{L_{\mathrm{M}}}{R}, \frac{t}{R}\right), \quad \bar{\sigma}_z = 0, \quad (26)$$

where the expression $H(L_{\mathrm{M}}/R, t/R)$ can be found in Eq. (A16) of Appendix II.

Then the elastic misfit energy U_{el} can be expressed as

$$U_{\mathrm{el}} = \frac{2\pi R t L_{\mathrm{M}} E\left(\varepsilon_1^{\mathrm{p}}\right)^2}{1-\nu} \cdot H\left(\frac{L_{\mathrm{M}}}{R}, \frac{t}{R}\right), \quad (27)$$

in which $H(L_{\mathrm{M}}/R, t/R)/(1-\nu)$ serves as the shape factor of the cylindrical domain.

Based on the above solution of the misfit strain energy U_{el} for an arbitrary tube wall-thickness/mean-radius ratio (ranging from 0 to 2), we perform a similar analysis as that in Sect. 3 to investigate the stability of domains in thick-walled tubes. The following demonstrates that the stability of a cylindrical martensite domain in tube configuration during displacement-controlled unloading is indeed governed by two nondimensional parameters, the tube length/mean-radius ratio L/R and the wall-thickness/mean-radius ratio t/R.

The variations of the critical domain length $L_{\mathrm{M}}^{\mathrm{c}}$ and the corresponding stress jump $\Delta\sigma$ with the wall-thickness/mean-radius ratio t/R are respectively shown in Figs. 9 and 10 for different tube length/mean-radius ratios L/R in the unloading process. It is seen that the critical martensite volume $L_{\mathrm{M}}^{\mathrm{c}}/R$ and stress jump $\Delta\sigma$ decreases monotonically as t/R decreases for a relatively large tube length/mean-radius ratio (i.e., $L/R > 20$). For a smaller tube length/mean-radius ratio such as $L/R = 10$, it can be seen that the variation of $L_{\mathrm{M}}^{\mathrm{c}}/R$ and $\Delta\sigma$ with t/R are non-monotonic with a local minimum value of $L_{\mathrm{M}}^{\mathrm{c}}/R \approx 0.5$ occurring at $t/R \approx 0.5$. This could be evidence of strong interaction among three nondimensional length scales, the normalized tube length L/R, the normalized wall-thickness t/R and the normalized critical domain length $L_{\mathrm{M}}^{\mathrm{c}}/R$. Moreover, for all values of t/R the critical martensite volume $L_{\mathrm{M}}^{\mathrm{c}}/R$ increases and the stress jump $\Delta\sigma$ decreases as the tube length L/R increases. The limiting case $L/R \to \infty$ gives the upper bound of the critical martensite volume $L_{\mathrm{M}}^{\mathrm{c}}/R$ and the lower bound of the stress jump ($\Delta\sigma = 0$).

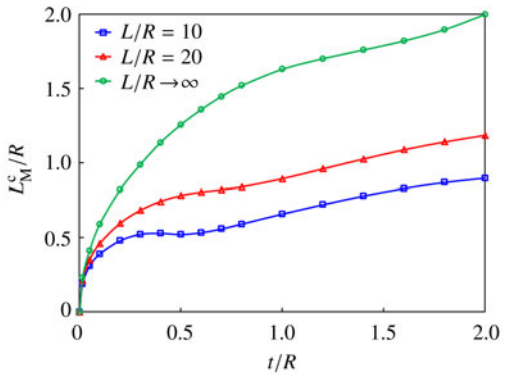

Fig. 9 Variation of the critical domain length L^c_M with the wall-thickness/mean-radius ratio t/R

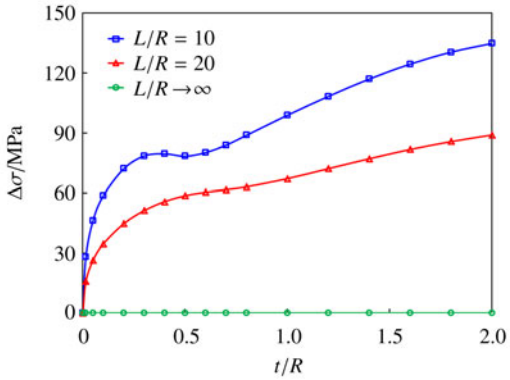

Fig. 10 Variation of the stress jump $\Delta\sigma$ with the wall-thickness/mean-radius ratio t/R

In summary, the effect of the wall-thickness/mean-radius ratio t/R on the critical domain length L^c_M and corresponding stress jump $\Delta\sigma$ is studied in this section as an extension of the effect of the tube-length/mean-radius ratio L/R in Sect. 3. Generally speaking, the critical domain length and corresponding stress jump increase as the wall-thickness/mean-radius ratio increases for a given tube length/mean-radius ratio.

5 Summary and Conclusions

The nominal stress-strain response of a superelastic NiTi tubes is one of the most important issues in its applications. During isothermal quasi-static tensile loading and unloading, the formation/vanishing of a domain in the tube are instability events accompanied by a rapid stress drop/rise. From a thermodynamic point of view, both domain formation and vanishing involve the unstable growth/shrinkage of the domain once the system reaches its critical state. Under the displacement-controlled unloading the domain front interaction (among many others factors such as defects, microstructure, external noise, etc.) plays an important role in the energetics of the unstable events when the two fronts are close to each other. In this paper, a quantitative study on domain vanishing was performed with focus on the domain front interaction in the stable→unstable transition. Starting from a cylindrical inclusion-matrix system, the energetics of the system and the stability of the domain were quantified. The main conclusions of this paper are drawn as follows.

(1) The front interaction of a cylindrical domain in long tubes depends on three length scales: the domain length, the mean-radius and the wall-thickness of the tube. The mean-radius and wall-thickness determine the characteristic length scale of the necking zone in the deformation of the tube, while the domain length determines the front interaction which occurs when the domain length becomes comparable to or less than the necking zone length.

(2) During isothermal displacement-controlled unloading, the shrinkage of a cylindrical domain of martensite phase is stable as long as the domain length is larger than the critical length. When the domain length is reduced to a critical length, the domain will become unstable and any small change in the domain length will lead to rapid domain vanishing due to the negative driving force at the domain fronts. The critical domain length (at the start of unstable domain vanishing) is determined by the tube length/mean-radius ratio and the wall-thickness/mean-radius ratio. For a given tube wall-thickness/mean-radius ratio, the longer the tube length, the longer the critical domain length and the smaller the stress jump at vanishing. Moreover, for a given tube length/mean-radius ratio, the critical domain length and corresponding stress jump increase as the wall-thickness/mean-radius ratio increases.

Appendix I

Consider a thin-walled tube with an overall necking deformation as shown in Fig. 2a. After section T_2 is disconnected from the rest of the tube (T_1 and T_3), section T_2 will have a uniform overall stress-free radial necking (see Fig. 2b). To connect T_1, T_2 and T_3, the shear force Q must be applied to the disconnected cross-sections (see Fig. 2c). The shear force results in bending of the tube in small regions near the joint line where they are applied. Let d be the dimension of such a region (so that its area is of the order of Rd). Since the deflection w of the tube mid-surface varies considerably over the distance d, the bending energy per unit area is of the order of Et^3w^2/d^4. Therefore the total bending energy (over an area $\sim Rd$) is

$$U_{\text{bend}} \sim ERt^3w^2/d^3. \tag{A1}$$

The strain for general mid-surface stretching is $\sim w/R$, and the stretching energy per unit area is of the order of Etw^2/R^2. Therefore the total stretching energy (over an area $\sim Rd$) due to the shear force Q is

$$U_{\text{stretch}} \sim Edtw^2/R. \tag{A2}$$

Since the bending energy increases and the stretching energy decreases with decreasing d, it is clear that both energies must be taken into account in determining the deformation near the line of application of the shear force Q. The size d of the necking (bending) zone is given in the order of magnitude by the condition that the sum of these energies is a minimum, when

$$d \sim \sqrt{Rt}. \tag{A3}$$

The total energy of the system can be expressed as

$$U_{\mathrm{el}} \sim Et^{3/2}w^2/R^{1/2}. \tag{A4}$$

Varying this with respect to w and equating the result to the work done by the shear force Q, we find the deflection $w \sim Q/(t/R)^{3/2}$.

Appendix II

AII 1 Sub-problem 1

In Sub-problem 1, the martensite domain (with constant eigenstrains $\varepsilon_r^{\mathrm{p}}$, $\varepsilon_\theta^{\mathrm{p}}$ and $\varepsilon_z^{\mathrm{p}}$) is subjected to the traction $p = -E\varepsilon_1^{\mathrm{p}}/(1-\nu) > 0$ on its inner and outer surfaces to guarantee that there is no radial deflection of the tube. The displacements of the cylindrical tube have the following forms

$$\begin{aligned}
&u_r^{\mathrm{I}} = 0, \quad u_z^{\mathrm{I}} = Az, \ \text{ for } \ |z| < \frac{L_{\mathrm{M}}}{2},\\
&u_r^{\mathrm{I}} = 0, \quad u_z^{\mathrm{I}} = \frac{AL_{\mathrm{M}}}{2}, \ \text{ for } \ z > \frac{L_{\mathrm{M}}}{2},\\
&u_r^{\mathrm{I}} = 0, \quad u_z^{\mathrm{I}} = -\frac{AL_{\mathrm{M}}}{2}, \ \text{ for } \ z < -\frac{L_{\mathrm{M}}}{2},\\
&u_r^{\mathrm{I}} = 0, \quad u_z^{\mathrm{I}} = -\frac{AL_{\mathrm{M}}}{2}, \ \text{ for } \ z < -\frac{L_{\mathrm{M}}}{2},
\end{aligned} \tag{A5}$$

with $A = 2\nu\varepsilon_1^{\mathrm{p}}/(1-\nu) + \varepsilon_2^{\mathrm{p}}$.

Accordingly the stresses in the tube are obtained from Eqs. (19) and (20) as

$$\begin{aligned}
&\sigma_r^{\mathrm{I}} = \sigma_\theta^{\mathrm{I}} = -\frac{E\varepsilon_1^{\mathrm{p}}}{1-\nu}, \quad \sigma_z^{\mathrm{I}} = \sigma_{rz}^{\mathrm{I}} = 0, \ \text{ for } \ |z| < \frac{L_{\mathrm{M}}}{2},\\
&\sigma_r^{\mathrm{I}} = \sigma_\theta^{\mathrm{I}} = \sigma_z^{\mathrm{I}} = \sigma_{rz}^{\mathrm{I}} = 0, \ \text{ for } \ |z| > \frac{L_{\mathrm{M}}}{2}.
\end{aligned} \tag{A6}$$

It is easy to check that the displacement in Eq. (A5) satisfies the governing Eq. (21), but it fails to satisfy the lateral boundary condition (22) for $|z| < L_{\mathrm{M}}/2$. Consider the force balance, the solution gives

$$\begin{aligned}
&\sigma_r^{\mathrm{I}}\big|_{r=R\pm t/2} = p = -\frac{E\varepsilon_1^{\mathrm{p}}}{1-\nu} > 0,\\
&\sigma_{rz}^{\mathrm{I}}\big|_{r=R\pm t/2} = 0, \ \text{ for } \ |z| < \frac{L_{\mathrm{M}}}{2},\\
&\sigma_r^{\mathrm{I}}\big|_{r=R\pm t/2} = \sigma_{rz}^{\mathrm{I}}\big|_{r=R\pm t/2} = 0, \ \text{ for } \ |z| > \frac{L_{\mathrm{M}}}{2}.
\end{aligned} \tag{A7}$$

AII 2 Sub-problem 2

In Sub-problem 2, the pure elastic tube is subjected to the distributed pressure $p = -E\varepsilon_1^{\mathrm{p}}/(1-\nu) > 0$ on its inner and outer surfaces over $|z| < L_{\mathrm{M}}/2$. The lateral boundary condition can be expressed as

$$\begin{aligned}
&\sigma_r^{\mathrm{II}}\big|_{r=R\pm t/2} = p, \quad \sigma_{rz}^{\mathrm{II}}\big|_{r=R\pm t/2} = 0, \ \text{ for } \ |z| < \frac{L_{\mathrm{M}}}{2},\\
&\sigma_r^{\mathrm{II}}\big|_{r=R\pm t/2} = \sigma_{rz}^{\mathrm{II}}\big|_{r=R\pm t/2} = 0, \ \text{ for } \ |z| > \frac{L_{\mathrm{M}}}{2}.
\end{aligned} \tag{A8}$$

A standard way to solve the axisymmetric elastic problem is to employ Love's stress function ϕ. The stress and displacement components can be expressed as

$$\begin{aligned}
\sigma_r^{\mathrm{II}} &= \frac{\partial}{\partial z}\left(\nu\nabla^2\phi - \frac{\partial^2\phi}{\partial r^2}\right),\\
\sigma_\theta^{\mathrm{II}} &= \frac{\partial}{\partial z}\left(\nu\nabla^2\phi - \frac{1}{r}\frac{\partial\phi}{\partial r}\right),\\
\sigma_z^{\mathrm{II}} &= \frac{\partial}{\partial z}\left[(2-\nu)\nabla^2\phi - \frac{\partial^2\phi}{\partial r^2}\right],\\
\sigma_{rz}^{\mathrm{II}} &= \frac{\partial}{\partial r}\left[(1-\nu)\nabla^2\phi - \frac{\partial^2\phi}{\partial z^2}\right],\\
u_r^{\mathrm{II}} &= -\frac{1+\nu}{E}\frac{\partial^2\phi}{\partial r\partial z},\\
u_z^{\mathrm{II}} &= \frac{1+\nu}{E}\left[2(1-\nu)\nabla^2\phi - \frac{\partial^2\phi}{\partial z^2}\right],
\end{aligned} \tag{A9}$$

where ϕ satisfies the bi-harmonic equation $\nabla^2\nabla^2\phi = 0$.

In order to satisfy the bi-harmonic equation, the stress function is assumed to be

$$\begin{aligned}
\phi = 2pR^3 \int_0^\infty \Big[&-\rho_1 kr' I_1(kr') + \rho_2 kr' K_1(kr')\\
&+ \rho_3 kr' I_0(kr') + \rho_4 kr' K_0(kr')\Big]\\
&\times \sin(kz')\sin\left(\frac{kL'_{\mathrm{M}}}{2}\right)\mathrm{d}k,
\end{aligned} \tag{A10}$$

where $r' = r/R$, $L'_{\mathrm{M}} = L_{\mathrm{M}}/R$ and $z' = z/R$. $I_0(kr')$ and $I_1(kr')$ are first kind modified Bessel functions of the zero and the first orders, respectively. $K_0(kr')$ and $K_1(kr')$ are second kind modified Bessel functions of the zero and the first orders, respectively.

From Eq. (A9), the stress and displacement components

can be expressed as

$$\begin{aligned}
\sigma_{rz}^{\mathrm{II}} = & \ 2p\int_0^\infty (\rho_1 M_{11}+\rho_2 M_{12}+\rho_3 M_{13}+\rho_4 M_{14}) \\
& \times k^3 \sin kz' \sin\frac{kL'_{\mathrm{M}}}{2}\mathrm{d}k, \\
\sigma_{r}^{\mathrm{II}} = & \ 2p\int_0^\infty (\rho_1 M_{21}+\rho_2 M_{22}+\rho_3 M_{23}+\rho_4 M_{24}) \\
& \times k^3 \cos kz' \sin\frac{kL'_{\mathrm{M}}}{2}\mathrm{d}k, \\
\sigma_{z}^{\mathrm{II}} = & \ 2p\int_0^\infty (\rho_1 M_{31}+\rho_2 M_{32}+\rho_3 M_{33}+\rho_4 M_{34}) \\
& \times k^3 \cos kz' \sin\frac{kL'_{\mathrm{M}}}{2}\mathrm{d}k, \\
\sigma_{\theta}^{\mathrm{II}} = & \ 2p\int_0^\infty (\rho_1 M_{41}+\rho_2 M_{42}+\rho_3 M_{43}+\rho_4 M_{44}) \\
& \times k^3 \cos kz' \sin\frac{kL'_{\mathrm{M}}}{2}\mathrm{d}k, \\
u_r^{\mathrm{II}} = & \ \frac{2(1+v)pR}{E}\int_0^\infty (\rho_1\chi_{11}+\rho_2\chi_{12}+\rho_3\chi_{13} \\
& +\rho_4\chi_{14})k^2 \cos kz' \sin\frac{kL'_{\mathrm{M}}}{2}\mathrm{d}k, \\
u_z^{\mathrm{II}} = & \ \frac{2(1+v)pR}{E}\int_0^\infty (\rho_1\chi_{21}+\rho_2\chi_{22}+\rho_3\chi_{23} \\
& +\rho_4\chi_{24})k^2 \sin kz' \sin\frac{kL'_{\mathrm{M}}}{2}\mathrm{d}k,
\end{aligned} \tag{A11}$$

where the expressions of M_{ij} and χ_{ij} are listed as

$$\begin{aligned}
&M_{11}(kr') = -kr' I_0(kr') - 2(1-v) I_1(kr'), \\
&M_{12}(kr') = -kr' K_0(kr') + 2(1-v) K_1(kr'), \\
&M_{13}(kr') = I_1(kr'), \\
&M_{14}(kr') = -K_1(kr'), \\
&M_{21}(kr') = (1-2v) I_0(kr') + kr' I_1(kr'), \\
&M_{22}(kr') = (1-2v) K_0(kr') - kr' K_1(kr'), \\
&M_{23}(kr') = -I_0(kr') + \frac{I_1(kr')}{kr'}, \\
&M_{24}(kr') = -K_0(kr') - \frac{K_1(kr')}{kr'}, \\
&M_{31}(kr') = -(4-2v) I_0(kr') - kr' I_1(kr'), \\
&M_{32}(kr') = -(4-2v) K_0(kr') + kr' K_1(kr'), \\
&M_{33}(kr') = I_0(kr'), \quad M_{34}(kr') = K_0(kr'), \\
&M_{41}(kr') = (1-2v) I_0(kr'), \\
&M_{42}(kr') = (1-2v) K_0(kr'), \\
&M_{43}(kr') = -\frac{I_1(kr')}{kr'}, \\
&M_{44}(kr') = \frac{K_1(kr')}{kr'}, \\
&\chi_{11}(kr') = kr' I_0(kr'), \\
&\chi_{12}(kr') = kr' K_0(kr'), \\
&\chi_{13}(kr') = -I_1(kr'), \\
&\chi_{14}(kr') = K_1(kr'), \\
&\chi_{21}(kr') = -4(1-v) I_0(kr') - kr' I_1(kr'), \\
&\chi_{22}(kr') = -4(1-v) K_0(kr') + kr' K_1(kr'), \\
&\chi_{23}(kr') = I_0(kr'), \\
&\chi_{24}(kr') = K_0(kr').
\end{aligned}$$

In order to satisfy the lateral boundary condition (AII4), the unknown functions ρ_1, ρ_2, ρ_3 and ρ_4 should be determined by the following equations (noting $t' = t/R$, $a' = 1 - t'/2$ and $b' = 1 + t'/2$)

$$\begin{aligned}
&\rho_1 M_{11}(ka') + \rho_2 M_{12}(ka') + \rho_3 M_{13}(ka') \\
&\quad +\rho_4 M_{14}(ka') = 0, \\
&\rho_1 M_{21}(ka') + \rho_2 M_{22}(ka') + \rho_3 M_{23}(ka') \\
&\quad +\rho_4 M_{24}(ka') = -\frac{1}{\pi k^4}, \\
&\rho_1 M_{11}(kb') + \rho_2 M_{12}(kb') + \rho_3 M_{13}(kb') \\
&\quad +\rho_4 M_{14}(kb') = 0, \\
&\rho_1 M_{21}(kb') + \rho_2 M_{22}(kb') + \rho_3 M_{23}(kb') \\
&\quad +\rho_4 M_{24}(kb') = -\frac{1}{\pi k^4},
\end{aligned} \tag{A12}$$

by using the relation

$$\int_0^\infty \frac{1}{k}\cos kz' \sin\frac{kL'_{\mathrm{M}}}{2}\mathrm{d}k = \begin{cases} \dfrac{\pi}{2}, & \text{for} \quad |z'| < \dfrac{L'_{\mathrm{M}}}{2} \\ 0, & \text{for} \quad |z'| > \dfrac{L'_{\mathrm{M}}}{2} \end{cases}. \tag{A13}$$

AII 3 Superposition of two sub-problems

By superposing the solutions of Sub-problems 1 and 2, we obtain the total displacements and stresses as

$$\begin{aligned}
&u_r = u_r^{\mathrm{I}} + u_r^{\mathrm{II}}, \quad u_z = u_z^{\mathrm{I}} + u_z^{\mathrm{II}}, \\
&\sigma_r = \sigma_r^{\mathrm{I}} + \sigma_r^{\mathrm{II}}, \quad \sigma_\theta = \sigma_\theta^{\mathrm{I}} + \sigma_\theta^{\mathrm{II}}, \\
&\sigma_z = \sigma_z^{\mathrm{I}} + \sigma_z^{\mathrm{II}}, \quad \sigma_{rz} = \sigma_{rz}^{\mathrm{I}} + \sigma_{rz}^{\mathrm{II}},
\end{aligned} \tag{A14}$$

which satisfy the basic equation (22) and boundary condition (23) of the original problem.

By substituting Eqs. (A6), (A11) and (A14) into Eq. (25), we obtain

$$\bar{\sigma}_r + \bar{\sigma}_\theta = \frac{2}{1-v} H(L'_{\mathrm{M}}, t'), \quad \bar{\sigma}_z = 0, \tag{A15}$$

where

$$H(L'_{\mathrm{M}}, t') = 1 + \frac{2}{L'_{\mathrm{M}} t'}\int_0^\infty (\rho_1 G_1 + \rho_2 G_2 + \rho_3 G_3 + \rho_4 G_4)$$

$$\times \sin^2 \frac{kL'_{\mathrm{M}}}{2} \mathrm{d}k. \tag{A16}$$

The expressions of G_i in Eq. (A16) are

$$\begin{aligned} G_1 &= 7\,(kb')^2\, I_0\,(kb') - 4vkb' I_1\,(kb') \\ &\quad - (ka')^2\, I_0\,(ka') + 4vka' I_1\,(ka')\,, \\ G_2 &= (kb')^2\, K_0\,(kb') + 4vkb' K_1\,(kb') \\ &\quad - (ka')^2\, K_0\,(ka') - 4vka' K_1\,(ka')\,, \\ G_3 &= -kb' I_1\,(kb') + ka' I_1\,(ka')\,, \\ G_4 &= kb' K_1\,(kb') - ka' K_1\,(ka')\,. \end{aligned} \tag{A17}$$

References

1 Otsuka, K., Wayman, C.M.: Shape Memory Materials. Cambridge University Press, Cambridge (1998)

2 Yoneyama, T., Miyazaki, S.: Shape Memory Alloys for Biomedical Applications. Woodhead Publishing Limited, Cambridge (2009)

3 Siddons, D.J., Moon, J.R.: Tensile and compression performance of superelastic NiTi tubing. Mater. Sci. Tech. **17**, 1073–1078 (2001)

4 Li, Z. Q., Sun, Q. P.: The initiation and growth of macroscopic martensite band in nano-grained NiTi microtube under tension. Int. J. Plast. **18**, 1481–1498 (2002)

5 Sun, Q. P., Li, Z. Q.: Phase transformation in superelastic NiTi polycrystalline micro-tubes under tension and torsion–from localization to homogeneous deformation. Int. J. Solids Struct. **39**, 3797–3809 (2002)

6 McNaney, J. M., Imbeni, V., Jung, Y., et al.: An experimental study of the superelastic effect in a shape-memory Nitinol alloy under biaxial loading. Mech. Mater. **35**, 969–986 (2003)

7 Matsui, R., Tobushi, H., Furuichi, Y., et al.: Tensile deformation and rotating-bending fatigue properties of a high elastic thin wire, a superelastic thin wire, and a superelastic thin tube of NiTi alloys. J. Engng. Mater. Tech. **126**, 384–391 (2004)

8 Ng, K. L., Sun, Q. P.: Stress-induced phase transformation and detwinning in NiTi polycrystalline shape memory alloy tubes. Mech. Mater. **38**, 41–56 (2006)

9 Feng P., Sun, Q. P.: In situ profilometry for non-uniform strain field measurement of NiTi shape memory alloy microtubing under complex stress states. Smart Mater. Struct. **16**, 179–186 (2007)

10 Feng, P., Sun, Q. P.: Experimental investigation on macroscopic domain formation and evolution in polycrystalline NiTi microtubing under mechanical force. J. Mech. Phys. Solids **54**, 1568–1603 (2006)

11 Favier, D., Louche, H., Schlosser, P., et al.: Homogeneous and heterogeneous deformation mechanisms in an austenitic polycrystalline Ti-50.8 at.% Ni thin tube under tension-investigation via temperature and strain fields measurements. Acta Mater. **55**, 5310–5322 (2007)

12 Grabe, C., Bruhns, O. T.: On the viscous and strain rate dependent behavior of polycrystalline NiTi. Int. J. Solids Struct. **45**, 1876–1895 (2008a)

13 Grabe, C., Bruhns, O. T.: Tension/torsion tests of pseudoelastic, polycrystalline NiTi shape memory alloys under temperature control. Mater. Sci. Engng.: A **481-482**, 109–113 (2008b)

14 Grabe, C., Bruhns, O. T.: Path dependence and multiaxial behavior of a polycrystalline NiTi alloy within the pseudoelastic and pseudoplastic temperature regimes. Int. J. Plast. **25**, 513–545 (2009)

15 He, Y. J., Sun, Q. P.: Effects of structural and material length scales on stress-induced martensite macro-domain patterns in tube configurations. Int. J. Solids Struct. **46**, 3045–3060 (2009)

16 He, Y. J., Sun, Q. P.: Scaling relationship on macroscopic helical domains in NiTi tubes. Int. J. Solids Struct. **46**, 4242–4251 (2009)

17 Zhou, R. H.: Macroscopic domain pattern selectrion in shape memory alloys: effects of length and time scales. [Ph.D. Thesis]. The Hong Kong University of Science and Technology Hongkong China (2011)

18 Leo, P. H., Shield, T. W., Bruno, O. P.: Transient heat transfer effects on the pseudoelastic behavior of shape-memory wires. Acta Metall. Mater. **41**, 2477–2485 (1993)

19 Bruno, O. P., Leo, P. H., Reitich, F.: Free boundary conditions at austenite-martensite interfaces. Phys. Rev. Lett. **74**, 746–749 (1995)

20 Shield, T. W., Leo, P. H., Grebner, W. C. C.: Quasi-static extension of shape memory wires under constant load. Acta Mater. **45**, 67–74 (1997)

21 Shaw, J. A., Kyriakides, S.: Thermomechanical aspects of NiTi. J. Mech. Phys. Solids **43**, 1243–1281 (1995)

22 Shaw, J. A., Kyriakides, S.: On the nucleation and propagation of phase transformation fronts in a NiTi alloy. Acta Mater. **45**, 683–700 (1997)

23 Tobushi, H., Shimeno, Y., Hachisuka, T., et al.: Influence of strain rate on superelastic properties of TiNi shape memory alloy. Mech. Mater. **30**, 141–150 (1998)

24 Iadicola, M. A., Shaw, J. A.: Rate and thermal sensitivities of unstable transformation behavior in a shape memory alloy. Int. J. Plast. **20**, 577–605 (2004)

25 Vitiello, A., Giorleo, G., Morace, R. E.: Analysis of thermomechanical behaviour of Nitinol wires with high strain rates. Smart Mater. Struct. **14**, 215–221 (2005)

26 Pieczyska, E. A., Gadaj, S. P., Nowacki, W. K., et al.: Phase-transformation fronts evolution for stress- and strain-controlled tension tests in TiNi shape memory alloy. Exp. Mech. **46**, 531–542 (2006)

27 He, Y. J., Sun, Q. P.: Rate-dependent domain spacing in a stretched NiTi strip. Int. J. Solids Struct. **47**, 2775–2783 (2010)

28 Zhang, X. H., Feng, P., He, Y. J., et al.: Experimental study on rate dependence of macroscopic domain and stress hysteresis in NiTi shape memory alloy strips. Int. J. Mech. Sci. **52**, 1660–1670 (2010)

29 Sun, Q. P., Zhong, Z.: An inclusion theory for the propagation of martensite band in NiTi shape memory alloy wires under tension. Int. J. Plast. **16**, 1169–1187 (2000)

30 Zhong, Z., Sun, Q. P., Tong, P.: On the elastic axisymmetric deformation of a rod containing a single cylindrical inclusion. Int. J. Solids Struct. **37**, 5934–5955 (2000)

31 Yu, X. B., Sun, Q. P., Zhong, Z.: Effect of elastic matrix constraint on the tensile deformation of NiTi superelastic fiber. Int.

J. Solids Struct. **41**, 2659–2683 (2004)

32 Mura, T.: Micromechanics of Defects in Solids, (2nd edn). Kluwer Academic Publishers, Dordrecht Netherlands Boston (1987)

33 Landau, L. D., Lifshitz, E. M.: Theory of Elasticity. Pergamon, Oxford (1986)

34 Cook, R. D., Young, W. C.: Advanced Mechanics of Materials, (2nd edn). Prentice-Hall, Englewood Cliffs, NJ (1999).

35 Eshelby, J. D.: The force on an elastic singularity. Phil. Trans. Roy. Soc. London A **224**, 87–112 (1951)

36 Eshelby, J. D.: Energy relations and the energy-momentum tensor in continuum mechanics. In: Kanninen MF, Adler WF, Rosefield AR, Jaffe RI (eds) Inelastic Behavior of Solids. McGraw-Hill. New York, 77–114 (1970)

37 Eshelby, J. D.: The elastic energy-momentum tensor. J. Elast. **5**, 321–335 (1975)

38 Knowles, J. K.: On the dissipation associated with equilibrium shocks in finite elasticity. J. Elast. **9**, 131–158 (1979)

39 Abeyaratne, R., Knowles, J. K.: On the driving traction acting on a surface of discontinuity in a continuum. J. Mech. Phys. Solids **40**, 345–360 (1990)

40 Maugin, G. A.: Material Inhomogeneities in Elasticity, (1st edn). Chapman and Hall, London New York (1993)

41 Fried, E., Gurtin, M.E.: Coherent solid-state phase transitions with atomic diffusion: a thermomechanical treatment. J. Stat. Phys. **95**, 1361-1427 (1999)

42 Gurtin, M.E.: Configurational Forces as Basic Concept of Continuum Physics. Springer, New York (2000)

43 Mueller, R., Kolling, S., Gross, D.: On configurational forces in context of the finite element method. Int. J. Numer. Meth. Engng. **53**, 1557–1574 (2002)

44 Gross, D., Kolling, S., Mueller, R., et al.: Configurational forces and their application in solid mechanics. Eur. J. Mech. A/Solids **22**, 669–692 (2003)

45 Dong, L., Sun, Q. P.: On equilibrium domains in superelastic NiTi tubes - helix versus cylinder. Int. J. Solids Struct. **49**, 1063–1076 (2012)

46 Rice, J. R.: Inelastic constitutive relations for solids: an internal-variable theory and its application to metal plasticity. J. Mech. Phys. Solids **19**, 433–455 (1971)

47 Cahn, J. W., Hilliard, J. E.: Free energy of a nonuniform system I. Interfacial free energy. J. Chem. Phys. **28**, 258–267 (1958)

48 Cahn, J. W.: On spinodal decomposition. Acta Metal. **9**, 795–801 (1961)